

Spin Versus Charge Density Wave Order in Graphene-like Systems

Y. Araki^{1,2} and G. W. Semeno²

¹*Department of Physics, The University of Tokyo, Tokyo 113-0033, Japan*

²*Department of Physics and Astronomy, University of British Columbia, Vancouver, British Columbia, Canada V6T 1Z1*

A variational technique is used to study sublattice symmetry breaking by strong on-site and nearest neighbor interactions in graphene. When interactions are strong enough to break sublattice symmetry, and with relative strengths characteristic of graphene, a charge density wave Mott insulator is favored over the spin density wave condensates. In the spin density wave condensate we find that introduction of a staggered on-site energy (quasiparticle mass) leads to a splitting of the fermi velocities and mass gaps of the quasiparticle spin states.

PACS numbers: 73.22.Pr, 71.10.Fd, 71.27.+a, 11.80.Fv

The possibility of gapping the spectrum of graphene, either by explicit¹ or spontaneous sublattice symmetry breaking², is an important fundamental and practical problem³. At the fundamental level, the question of spontaneous breaking of either exact or approximate chiral symmetry emulates similar issues in quantum field theories such as quantum chromodynamics. At the practical level, a small gap, particularly one which could be switched on and off would be important for using graphene in electronics technology as it could give a mechanism for controlling the flow of electrons.

In the absence of magnetic fields, the best clean, suspended graphene is a semi-metal with no discernible energy gap. Gap formation by spontaneous symmetry breaking, if it occurred, would be driven by strong electron-electron interactions. Numerical Monte Carlo computations and series expansions of the Hubbard model on a hexagonal lattice indicate that a phase transition from a semi-metal to an anti-ferromagnetic, or spin density wave (SDW), Mott insulator⁴⁻⁶ (with perhaps other exotic phases in between) will occur for relatively strong coupling, $U/t \sim 3-5$, where U is the on-site Hubbard interaction and t is the hopping parameter. Estimates of these parameters for suspended graphene, where an on-site Coulomb energy is $U \sim 10\text{eV}$ and $t = 2.7\text{eV}$ have a ratio in the same range, raising the tantalizing idea that graphene is close to this critical point and some small modification which enhances the interaction could induce a phase transition to a gapped state^{3,7-10}. The simplest gapped states are spin density wave and charge density wave (CDW) Mott insulators, although more exotic phases have been discussed^{6,11-14}. There is also a possibility of breaking the sublattice symmetry explicitly by depositing graphene on the appropriate substrate, such as boron nitride or silicon carbide^{1,9,15}. Even once it is broken explicitly, there can be phase transition between different patterns, for example CDW to SDW, which can be of great interest. Moreover, the interplay between spontaneous and explicit symmetry breaking is an interesting problem which has been discussed in recent literature¹⁶⁻¹⁸.

In this Letter, we shall show that, even with explicit symmetry breaking, electron-electron interactions can

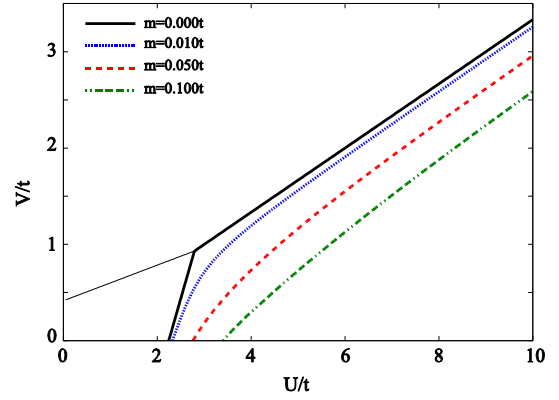


FIG. 1: The phase diagram of the extended Hubbard model with staggered potential m . The thick lines are phase boundaries between the SDW phase ($\text{sgn}\Delta_{\uparrow} = -\text{sgn}\Delta_{\downarrow}$) and the SM/CDW phase ($\text{sgn}\Delta_{\uparrow} = \text{sgn}\Delta_{\downarrow}$), while the thin line for $m = 0$ is the boundary between the SM and the CDW phases. The SM phase does not appear when m is finite. As m becomes larger, the SDW phase is suppressed.

change the character of the gap and the electron spectrum significantly. For example, a candidate for the gapped phase is an antiferromagnetic SDW Mott insulator, and it is indeed what is found in the Hubbard model at strong coupling⁴⁻⁶. We shall show that, when next-to-nearest neighbor (NN) interactions are added to the Hubbard model, with the strength appropriate to graphene ($V \sim 10\text{eV}$), a CDW state is favored over the antiferromagnetic SDW. A quantum phase transition between the two can be driven by varying either the strength of the NN coupling or the amplitude of an explicit symmetry breaking staggered potential. Our central result is the phase diagram in Fig. 1. The critical Hubbard coupling is underestimated by our technique, likely because magnon fluctuations are not taken into account. In the absence of explicit symmetry breaking, the semi-metal phase occurs in the trapezoid in the lower left-hand corner.

We shall use a variational technique where we replace the full Hamiltonian H by a solvable trial Hamiltonian

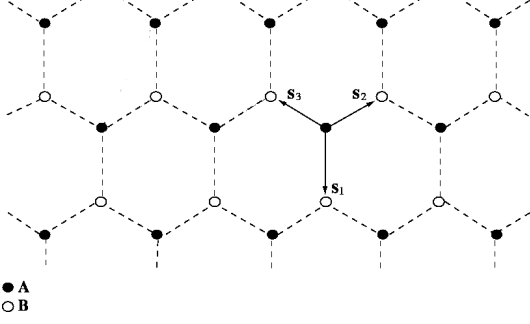


FIG. 2: The hexagonal graphene lattice composed of sublattices A (black dots) and B (white dots) connected by the basis vectors \mathbf{s}_i .

H_0 which is optimized using Jensen's inequality¹⁹,

$$F \leq F_0 + \langle H - H_0 \rangle_0. \quad (1)$$

We shall adjust H_0 to minimize this upper bound on the free energy. Here, $\langle \mathcal{O} \rangle_0 = \text{Tr} e^{-\beta H_0} \mathcal{O} / \text{Tr} e^{-\beta H_0}$.

For the Hamiltonian of graphene, we begin with the tight-binding model with nearest-neighbor (NN) hopping.

$$H_T = -t \sum_{i, \sigma, \mathbf{r} \in A} [a_{\sigma}^{\dagger}(\mathbf{r}) b_{\sigma}(\mathbf{r} + \mathbf{s}_i) + b_{\sigma}^{\dagger}(\mathbf{r} + \mathbf{s}_i) a_{\sigma}(\mathbf{r})]. \quad (2)$$

The hexagonal graphene lattice is depicted in Fig. 2. It contains two triangular sublattices, A and B. Creation and annihilation operators for electrons at sites \mathbf{r} on sublattice A are $(a_{\sigma}^{\dagger}(\mathbf{r}), a_{\sigma}(\mathbf{r}))$ and B are $(b_{\sigma}^{\dagger}(\mathbf{r}), b_{\sigma}(\mathbf{r}))$. $\sigma = \uparrow, \downarrow$ is the spin index. We shall add a staggered on-site energy, H_M , which models explicit sublattice symmetry breaking (which could arise by interaction with a substrate, for example, and gives the low energy graphene Dirac electron a mass gap²⁰), a Hubbard interaction H_U and a NN interaction H_V ,

$$H_M = m \sum_{\mathbf{r} \in A} [b_{\sigma}^{\dagger}(\mathbf{r} + \mathbf{s}_1) b_{\sigma}(\mathbf{r} + \mathbf{s}_1) - a_{\sigma}^{\dagger}(\mathbf{r}) a_{\sigma}(\mathbf{r})] \quad (3)$$

$$H_U = \frac{U}{2} \left[\sum_{\mathbf{r} \in A} (a_{\sigma}^{\dagger}(\mathbf{r}) a_{\sigma}(\mathbf{r}) - 1)^2 + \sum_{\mathbf{r} \in B} (b_{\sigma}^{\dagger}(\mathbf{r}) b_{\sigma}(\mathbf{r}) - 1)^2 \right] \quad (4)$$

$$H_V = V \sum_{\mathbf{r} \in A, i} [a_{\sigma}^{\dagger}(\mathbf{r}) a_{\sigma}(\mathbf{r}) - 1] [b_{\sigma'}^{\dagger}(\mathbf{r} + \mathbf{s}_i) b_{\sigma'}(\mathbf{r} + \mathbf{s}_i) - 1] \quad (5)$$

where terms such as $a_{\sigma}^{\dagger}(\mathbf{r}) a_{\sigma}(\mathbf{r})$ are summed over spins. An important symmetry of graphene which is to a good approximation visible in angle-resolved photoemission spectroscopy (ARPES) measurements²¹ is particle-hole symmetry. Here, we have written a model Hamiltonian $H = H_T + H_M + H_U + H_V$ which has exact particle-hole symmetry. We will also restrict the variational Ansatz to have this symmetry. The explicit

particle-hole transformation is $a_{\sigma}^{\dagger}(\mathbf{r}), a_{\sigma}(\mathbf{r}), b_{\sigma}^{\dagger}(\mathbf{r}), b_{\sigma}(\mathbf{r}) \rightarrow a_{\sigma}(\mathbf{r}), a_{\sigma}^{\dagger}(\mathbf{r}), -b_{\sigma}(\mathbf{r}), -b_{\sigma}^{\dagger}(\mathbf{r})$. The terms in the Hamiltonian H_T, H_U, H_V, H_M are invariant.

To write down the trial Hamiltonian H_0 , it is convenient to Fourier transform to momentum space where

$$H_0 = \sum_{\mathbf{k}, \sigma} (a_{\sigma}^{\dagger}(\mathbf{k}), b_{\sigma}^{\dagger}(\mathbf{k})) \begin{pmatrix} \Delta_{\sigma}(\mathbf{k}) & h_{\sigma}(\mathbf{k}) \\ h_{\sigma}^*(\mathbf{k}) & -\Delta_{\sigma}(\mathbf{k}) \end{pmatrix} \begin{pmatrix} a_{\sigma}(\mathbf{k}) \\ b_{\sigma}(\mathbf{k}) \end{pmatrix}, \quad (6)$$

where \mathbf{k} is a wave-vector in the Brillouin zone of the triangular lattice, and, for example

$$a(\mathbf{k}) = \sum_{\mathbf{r} \in A} \frac{e^{i\mathbf{k} \cdot \mathbf{r}}}{\sqrt{\Omega}} a_{\sigma}(\mathbf{r}), \quad a_{\sigma}(\mathbf{r}) = \int d\mathbf{k} \frac{e^{-i\mathbf{k} \cdot \mathbf{r}}}{\sqrt{\Omega}} a_{\sigma}(\mathbf{k}) \quad (7)$$

with Ω the volume of the Brillouin zone. Here we assume that the different matrix elements in the Hamiltonian can be simultaneously diagonalized in spin. This is not the most general possible Ansatz, which would have a more complicated spin dependence. We have assumed translation invariance on the triangular sublattices. If we set $\Delta_{\sigma}(\mathbf{k}) = 0$ and $h_{\sigma}(\mathbf{k}) = \sum e^{i\mathbf{k} \cdot \mathbf{s}_i} \equiv \Phi(\mathbf{k})$, H_0 becomes identical to the tight-binding model Hamiltonian H_T . We have fixed the diagonal parts of H_0 so that it has particle-hole symmetry. Aside from particle-hole symmetry, H_T, H_U, H_V also have sublattice symmetry – where we simply interchange the sublattice excitations $a_{\sigma}^{\dagger}(\mathbf{k}), a_{\sigma}(\mathbf{k}), b_{\sigma}^{\dagger}(\mathbf{k}), b_{\sigma}(\mathbf{k}) \rightarrow b_{\sigma}^{\dagger}(-\mathbf{k}), b_{\sigma}(-\mathbf{k}), a_{\sigma}^{\dagger}(-\mathbf{k}), a_{\sigma}(-\mathbf{k})$. This symmetry is broken by H_M , which flips sign under the transformation. The trial Hamiltonian has this symmetry only when $\Delta_{\sigma} = 0$. Hermiticity requires that $h_{\sigma}^*(-\mathbf{k}) = h_{\sigma}(\mathbf{k})$ and $\Delta_{\sigma}(\mathbf{k}) = \Delta_{\sigma}(-\mathbf{k}) = \text{real}$.

The spectrum and the eigenstates of H_0 are easy to find: The eigenvalues of the single-particle Hamiltonian are $E_{\sigma, \pm}(\mathbf{k}) \equiv \pm E_{\sigma}(\mathbf{k}) = \pm \sqrt{\Delta_{\sigma}(\mathbf{k})^2 + |h_{\sigma}(\mathbf{k})|^2}$. With a change of variables into polar coordinate $h = E \cos \theta e^{i\phi}$, $\Delta = E \sin \theta$ ($-\pi/2 \leq \theta \leq \pi/2$, $-\pi < \phi \leq \pi$), H_0 is diagonalized by the canonical transformation

$$a = \frac{1}{\sqrt{2(1 + \sin \theta)}} [(1 + \sin \theta) \psi_+ - \cos \theta e^{i\phi} \psi_-] \quad (8)$$

$$b = \frac{1}{\sqrt{2(1 + \sin \theta)}} [\cos \theta e^{-i\phi} \psi_+ + (1 + \sin \theta) \psi_-], \quad (9)$$

where we have suppressed \mathbf{k}, σ labels, and (ψ_+, ψ_-) and (ψ_+, ψ_-) are creation and annihilation operators for electrons in energy states $+E_{\sigma}(\mathbf{k})$ and $-E_{\sigma}(\mathbf{k})$, respectively. With this transformation, the correlation functions are diagonal in momentum and spin space,

$$\langle a_{\sigma}^{\dagger}(\mathbf{k}) a_{\sigma}(\mathbf{k}) \rangle_0 = \frac{1}{2} \left[1 - \sin \theta_{\sigma}(\mathbf{k}) \tanh \frac{\beta}{2} E_{\sigma}(\mathbf{k}) \right] \quad (10)$$

$$\langle b_{\sigma}^{\dagger}(\mathbf{k}) b_{\sigma}(\mathbf{k}) \rangle_0 = \frac{1}{2} \left[1 + \sin \theta_{\sigma}(\mathbf{k}) \tanh \frac{\beta}{2} E_{\sigma}(\mathbf{k}) \right] \quad (11)$$

$$\langle b_{\sigma}^{\dagger}(\mathbf{k}) a_{\sigma}(\mathbf{k}) \rangle_0 = -\frac{1}{2} \cos \theta_{\sigma}(\mathbf{k}) e^{i\phi_{\sigma}(\mathbf{k})} \tanh \frac{\beta E_{\sigma}(\mathbf{k})}{2} \quad (12)$$

All the others can be obtained from these by simple algebra. All expectation values of operators factor into

bilinears such as these. Then, the free energy per unit volume is the sum of the following five contributions, which come from $F_0 - \langle H_0 \rangle_0$ and the expectation values of H_T, H_M, H_U, H_V , respectively:

$$\epsilon_0 = \int \frac{d\mathbf{k}}{\Omega} \sum_{\sigma} \left[E_{\sigma}(\mathbf{k}) \tanh \frac{\beta E_{\sigma}(\mathbf{k})}{2} - \frac{2}{\beta} \ln \left[2 \cosh \frac{\beta E_{\sigma}(\mathbf{k})}{2} \right] \right] \quad (13)$$

$$\epsilon_T = \frac{t}{2} \int \frac{d\mathbf{k}}{\Omega} \sum_{\sigma} \cos \theta_{\sigma}(\mathbf{k}) e^{i\phi_{\sigma}(\mathbf{k})} \Phi(\mathbf{k}) \tanh \frac{\beta}{2} E_{\sigma}(\mathbf{k}) + \text{c.c.} \quad (14)$$

$$\epsilon_M = m \int \frac{d\mathbf{k}}{\Omega} \sum_{\sigma} \sin \theta_{\sigma}(\mathbf{k}) \tanh \frac{\beta}{2} E_{\sigma}(\mathbf{k}) \quad (15)$$

$$\epsilon_U = \frac{U}{4} \left[\sum_{\sigma} \int \frac{d\mathbf{k}}{\Omega} \sin \theta_{\sigma}(\mathbf{k}) \tanh \frac{\beta}{2} E_{\sigma}(\mathbf{k}) \right]^2 - \frac{U}{4} \sum_{\sigma} \left[\int \frac{d\mathbf{k}}{\Omega} \sin \theta_{\sigma}(\mathbf{k}) \tanh \frac{\beta}{2} E_{\sigma}(\mathbf{k}) \right]^2 \quad (16)$$

$$\epsilon_V = -\frac{3V}{4} \left[\sum_{\sigma} \int \frac{d\mathbf{k}}{\Omega} \sin \theta_{\sigma}(\mathbf{k}) \tanh \frac{\beta}{2} E_{\sigma}(\mathbf{k}) \right]^2 - \frac{V}{12} \sum_{\sigma} \left| \int \frac{d\mathbf{k}}{\Omega} \cos \theta_{\sigma}(\mathbf{k}) e^{i\phi_{\sigma}(\mathbf{k})} \Phi(\mathbf{k}) \tanh \frac{\beta}{2} E_{\sigma}(\mathbf{k}) \right|^2 \quad (17)$$

First, consider the equation obtained from varying $\phi_{\sigma}(\mathbf{k})$:

$$0 = Z_{\sigma} e^{i\phi_{\sigma}(\mathbf{k})} \Phi(\mathbf{k}) - Z_{\sigma}^* e^{-i\phi_{\sigma}(\mathbf{k})} \Phi^*(\mathbf{k}), \quad (18)$$

where the factor Z_{σ} is defined by

$$Z_{\sigma} = 1 - \frac{V}{6t} \int \frac{d\mathbf{k}}{\Omega} \cos \theta_{\sigma}(\mathbf{k}) e^{-i\phi_{\sigma}(\mathbf{k})} \Phi(\mathbf{k}) \tanh \frac{\beta}{2} E_{\sigma}(\mathbf{k}). \quad (19)$$

The solution of this equation which minimizes the energy is $\phi_{\sigma}(\mathbf{k}) = -\arg \Phi(\mathbf{k}) + \pi$. Thus, everywhere in Eqs. (13)-(17), $e^{i\phi} \Phi$ can be replaced by $-|\Phi|$. The equation obtained by varying $E_{\sigma}(\mathbf{k})$ and $\theta_{\sigma}(\mathbf{k})$ are

$$E_{\sigma}(\mathbf{k}) = \cos \theta_{\sigma}(\mathbf{k}) Z_{\sigma} t |\Phi(\mathbf{k})| + \left[\frac{3V}{2} C_{\sigma} - m + \frac{3V-U}{2} C_{\bar{\sigma}} \right] \sin \theta_{\sigma}(\mathbf{k}), \quad (20)$$

$$Z_{\sigma} t |\Phi(\mathbf{k})| \tan \theta_{\sigma}(\mathbf{k}) = \frac{3V}{2} C_{\sigma} - m + \frac{3V-U}{2} C_{\bar{\sigma}}, \quad (21)$$

where

$$C_{\sigma} = \int \frac{d\mathbf{k}}{\Omega} \sin \theta_{\sigma}(\mathbf{k}) \tanh \frac{\beta}{2} E_{\sigma}(\mathbf{k}) \quad (22)$$

$$Z_{\sigma} = 1 + \frac{V}{6t} \int \frac{d\mathbf{k}'}{\Omega} \cos \theta_{\sigma}(\mathbf{k}') |\Phi(\mathbf{k}')| \tanh \frac{\beta}{2} E_{\sigma}(\mathbf{k}'). \quad (23)$$

The solution reads

$$E_{\sigma}(\mathbf{k}) = \sqrt{Z_{\sigma}^2 t^2 |\Phi(\mathbf{k})|^2 + \left[\frac{3V}{2} C_{\sigma} - m + \frac{3V-U}{2} C_{\bar{\sigma}} \right]^2} \quad (24)$$

$$\sin \theta_{\sigma}(\mathbf{k}) = \left[\frac{3V}{2} C_{\sigma} - m + \frac{3V-U}{2} C_{\bar{\sigma}} \right] / E_{\sigma}(\mathbf{k}) \quad (25)$$

$$\cos \theta_{\sigma}(\mathbf{k}) = Z_{\sigma} t |\Phi(\mathbf{k})| / E_{\sigma}(\mathbf{k}), \quad (26)$$

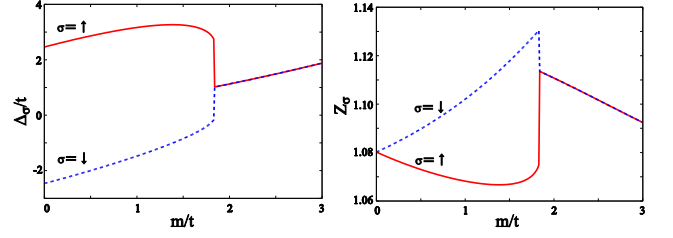


FIG. 3: The behavior of the density wave amplitude Δ_{σ} (left) and the velocity renormalization factor Z_{σ} (right) as functions of the external mass m , where the on-site interaction $U = 6.0t$ and the NN interaction $V = 0.5t$ are fixed. The system shows the SDW phase for $m < 1.8t$, while it reveals the CDW phase for $m > 1.8t$. The fermi velocity of the up spin and that of the down spin differ (i.e. $Z_{\uparrow} \neq Z_{\downarrow}$) in the SDW phase, unless $m = 0$.

The four constants C_{σ} and Z_{σ} must be determined self-consistently. Z_{σ} corrects the fermi velocity and C_{σ} and m gap the spectrum. If m were zero, but C_{σ} nonzero, the sublattice symmetry would be spontaneously broken. The nonzero temperature is important for deriving the variational equations, however, to study the low temperature limit, we will set it to zero.

Since, from Eq. (16), $\epsilon_U = \frac{U}{2} C_{\uparrow} C_{\downarrow}$, the Hubbard interaction favors a spin density wave (SDW) where C_{\uparrow} and C_{\downarrow} are nonzero and have opposite signs. From Eq. (17), $\epsilon_V = -\frac{3V}{4} (C_{\uparrow} + C_{\downarrow})^2 - 3V[(Z_{\uparrow} - 1)^2 + (Z_{\downarrow} - 1)^2]$. The NN interaction favors a charge density wave (CDW) where C_{\uparrow} and C_{\downarrow} are nonzero and have the same sign. The competition of these two phases is seen in the numerical solutions of the self-consistent equations, Eqs. (20)-(26). The phase diagram is shown in Fig. 1. When $m = 0$, there are three phases: a semi-metal (SM) for $U, V \lesssim t$, SDW for $U \gtrsim V, m$, and CDW for $V, m \gtrsim U$. H_M is a source for CDW. When it is finite, there is no SM phase. The SDW phase is suppressed as m increases, while the CDW phase is enhanced.

Now we shall investigate the quantitative behavior of Δ_{σ} and Z_{σ} , by varying one parameter out of U, V, m while holding the others fixed. We begin with $U = 6.0t, V = 0.5t, m = 0$, where the system is in the SDW phase, and we increase m . As shown in the left panel of Fig. 3, both Δ_{\uparrow} and Δ_{\downarrow} increase as a function of m as long as m is sufficiently small. It should be noted that $|\Delta_{\uparrow}|$ and $|\Delta_{\downarrow}|$ take different values in this region unless $m = 0$, which means that the quasiparticle gap for up spin and that for down spin are different. Such a discrepancy of $|\Delta_{\sigma}|$ also causes the discrepancy of the factor Z_{σ} through Eq.(23), as shown in the right panel of Fig.3. The difference between Z_{\uparrow} and Z_{\downarrow} increases as a function of m towards its maximum value $Z_{\downarrow} - Z_{\uparrow} = 0.05$ at $m = 1.7t$, then drastically drops towards zero at the critical value $m_C = 1.8t$. Since $\Delta_{\uparrow} = \Delta_{\downarrow}$ in the CDW region, quasiparticles with up spin and those with down spin obtain the same Fermi velocity above m_C .

Next we vary the NN interaction V , where the on-site interaction $U = 6.0t$ and the mass $m = 0.5t$ are fixed.

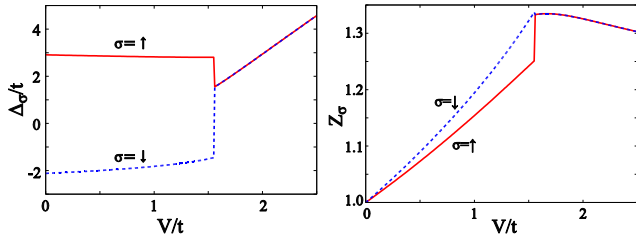


FIG. 4: The behavior of the density wave amplitude Δ_σ (left) and the velocity renormalization factor Z_σ (right) as functions of the NN interaction V , where the on-site interaction $U = 6.0t$ and the external mass $m = 0.5t$ are fixed. The system shows the SDW phase for $V < 1.5t$, while it reveals the CDW phase for $V > 1.5t$. The fermi velocity of the up spin and that of the down spin differ (i.e. $Z_\uparrow \neq Z_\downarrow$) in the SDW phase, unless $V = 0$.

The SDW amplitude is suppressed as V increases, and a phase transition to the CDW phase occurs at $V_C = 1.5t$, as shown in the left panel of Fig.4. Due to the finite external mass, m , there is a discrepancy between $|\Delta_\uparrow|$ and $|\Delta_\downarrow|$ in the SDW phase, which leads to the discrepancy between Z_\uparrow and Z_\downarrow , as shown in the right panel of Fig.4. Since $Z_\sigma - 1$ is proportional to V , Z_\uparrow and Z_\downarrow take the identical value (unity) at $V = 0$, even though the quasiparticle gap amplitudes are different. $Z_\downarrow - Z_\uparrow$ reaches its maximum value 0.09 just below the critical value V_C .

In conclusion, we note that, in the continuum limit of graphene, the CDW and SDW condensates are indistinguishable as they are related to each other by a transformation in the emergent $U(4)$ symmetry. We have found that they are indeed distinguished by lattice scale physics which can have an important effect. We have shown that the short ranged interactions of relative strengths approximating graphene favor the CDW state. This is basically due to the fact that the on-site energy is anomalously small compared to the NN potential energy. Explicit symmetry breaking, which can be present in some

cases enhances this effect. The conclusion that lattice scale physics can drive a phase transition is surprising. It is likely that the naive continuum Coulomb interaction is good for the semi-metal phase, however when density wave order sets in, it is driven by otherwise irrelevant four-Fermion interactions which can have nontrivial strong coupling fixed points. This point of view is supported by renormalization group analyses of the continuum theory²². Another anomalous effect of explicit symmetry breaking is the splitting of the Fermi velocities of the spin up and spin down electrons in the SDW phase. That splitting goes to zero if m goes to zero. It increases as a function of the NN interaction strength, and it reaches about 10% of the Fermi velocity. Such a discrepancy might be detected by ARPES measurements, and it may influence transport properties of the system.

Some of our results are similar to a self-consistent mean field theory. We point out that the variational technique is more general in that it contains a wave-function renormalization, which is normally absent in mean field approach. It is also readily applicable to a much wider array of potentials, and we believe that our exposition of the technique here could be used as a starting point for more general analyses of graphene-like systems. We have focused on the SDW and CDW patterns, but the honeycomb lattice can have a richer array of symmetry breaking patterns, such as the Kekulé distortion which is expected to become relevant when the next-to-NN interaction is taken into account. The interplay of ordering patterns including those phases, induced either spontaneously or explicitly, remains an open question.

Acknowledgments

Y. A. is supported by Grant-in-Aid for Japan Society for the Promotion of Science (DC1, No.22.8037). G.W.S. is supported by NSERC of Canada.

-
- ¹ K. Novoselov, Nature Materials **6**, 720 (2007).
 - ² G. W. Semenoff, Phys. Scr. **T146**, 014016 (2012).
 - ³ A. H. Castro Neto, Physics **2**, 30 (2009).
 - ⁴ S. Sorella, E. Tosatti, Europhys. Lett. **19**, 699 (1992).
 - ⁵ T. Paiva, R. T. Scalettar, W. Zheng, R. R. P. Singh, J. Oitmaa, Phys. Rev. B **72**, 085123 (2005).
 - ⁶ Z. Y. Meng, T. C. Lang, S. Wessel, F. F. Assaad, A. Muramatsu, Nature **464**, 847 (2010).
 - ⁷ I. F. Herbut, Phys. Rev. Lett. **97**, 146401 (2006).
 - ⁸ J. E. Drut, T. A. Lähde, Phys. Rev. Lett. **102**, 026802 (2009).
 - ⁹ S. Y. Zhou, G. H. Gweon, A. V. Fedorov, P. N. First, W. A. de Heer, D. H. Lee, F. Guinea, A. H. Castro Neto, A. Lanzara, Nature Materials **6**, 770 (2007).
 - ¹⁰ R. M. Ribeiro, V. M. Pereira, N. M. R. Peres, P. R. Bridgdon, A. H. Castro Neto, New J. Phys. **11**, 115002 (2009).
 - ¹¹ I. F. Herbut, V. Juricic, O. Vafek, Phys. Rev. B **80** 075432 (2009).
 - ¹² C. Chamon, C-Y. Hou, C. Mudry, S. Ryu, L. Santos, Phys. Scr. **T146**, 014013 (2012).
 - ¹³ S. Raghu, X.-L. Qi, C. Honerkamp and S.-C. Zhang, Phys. Rev. Lett. **100**, 156401 (2008).
 - ¹⁴ A.H. MacDonald, J. Jung, and F. Zhang, Phys. Scr. **T146**, 014012 (2012).
 - ¹⁵ G. Giovannetti, P. A. Khomyakov, G. Brocks, P. J. Kelly, J. van den Brink, Phys. Rev. B **76**, 073103 (2007).
 - ¹⁶ R. Dillenschneider, Phys. Rev. B **78**, 115417 (2008).
 - ¹⁷ Y. Araki, Phys. Rev. B **84**, 113402 (2011).
 - ¹⁸ D. Soriano, J. Fernández-Rossier, arXiv:1112.6334.
 - ¹⁹ J. L. W. V. Jensen, Acta Math **30** (1): 175.93 (1906).
 - ²⁰ G.W. Semenoff, Phys. Rev. Lett. **53**, 2449 (1984).
 - ²¹ D.A. Siegel, C.-H. Park, C. Hwang, J. Deslippe, A.V. Fedorov, S.G. Louie, A. Lanzara, Proc. Natl. Acad. Sci. USA **108**, 11365 (2011).

- ²² V. Juricic, I. F. Herbut, G. W. Semenoff, Phys. Rev. B **80**, 081405 (2009).